

Hierarchy of modes in an interacting system

O. Tsypliyatyev and A. J. Schofield

School of Physics and Astronomy, University of Birmingham, Birmingham, B15 2TT, UK

Y. Jin, M. Moreno, W. K. Tan, C. J. B. Ford, J. P. Griffiths, I. Farrer, G. A. C. Jones, and D. A. Ritchie
Cavendish Laboratory, University of Cambridge, J J Thomson Avenue, Cambridge, CB3 0HE, UK

(Dated: November 7, 2021)

Studying interacting fermions in 1D at high energy, we find a hierarchy in the spectral weights of the excitations theoretically and we observe evidence for second-level excitations experimentally. Diagonalising a model of fermions (without spin), we show that levels of the hierarchy are separated by powers of \mathcal{R}^2/L^2 , where \mathcal{R} is a length-scale related to interactions and L is the system length. The first-level (strongest) excitations form a mode with parabolic dispersion, like that of a renormalised single particle. The second-level excitations produce a singular power-law line shape to the first-level mode and multiple power-laws at the spectral edge. We measure momentum-resolved tunneling of electrons (fermions with spin) from/to a wire formed within a GaAs heterostructure, which shows parabolic dispersion of the first-level mode and well-resolved spin-charge separation at low energy with appreciable interaction strength. We find structure resembling the second-level excitations, which dies away quite rapidly at high momentum.

PACS numbers: 71.10.Pm, 03.75.Kk, 73.63.Nm, 73.90.+f

Identifying patterns within the spectrum of interacting quantum systems is notoriously hard and has often been limited to low-energy/low-momentum excitations (such as the Fermi-liquid [1] or Luttinger-liquid [2] descriptions). In this Letter we demonstrate, theoretically and supported by experiment, that a hierarchy of modes can emerge in interacting 1D systems controlled by system length. The dominant mode for long systems is a renormalized single-particle-like excitation which extends to high energies and momenta. This contrasts with the well-known and distinctly non-free-particle-like description of 1D systems at low energy. We show how these two regimes are connected.

Our method is the diagonalization of a model of spinless fermions with short-range interactions and the evaluation of its spectral function via Bethe ansatz methods. We find that the spectral weights of excitations have factors with different powers of a ratio of lengths, \mathcal{R}^2/L^2 , (which will be defined below) separating them into a hierarchy. The dispersion of the mode formed by excitations with zero power (which we call the first level) is parabolic with a mass renormalised by the Luttinger parameter K . The continuous spectrum of the second-level excitations produces a power-law line-shape around the first-level mode with a singular exponent -1 . The particle edge $p0b$ in Fig. 1 is a second-level mode with a different power-law behaviour of the spectral function from that of the first-level mode $h0a$ of the hole edge, with an exponent that coincides with the mobile-impurity model [3, 4]. The local density of states is dominated by the first-level excitations, producing a $1/\sqrt{\varepsilon}$ Van Hove singularity, where ε is the energy measured from the bottom of the conduction band, on the $\varepsilon > 0$ side. For $\varepsilon < 0$, the second-level excitations give the same $1/\sqrt{|\varepsilon|}$ singularity

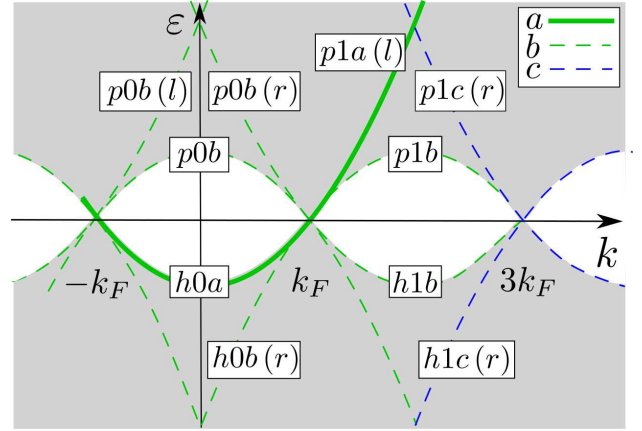


Figure 1. The main features of spectral function for spinless fermions in the region $-k_F < k < k_F$ ($k_F < k < 3k_F$) labelled by 0 (1). The grey area marks non-zero values, p (h) shows the particle(hole) sector, a , b , c respectively identify the level in the hierarchy in powers 0, 1, 2 of \mathcal{R}^2/L^2 , and (r, l) specifies the origin in the range—modes on the edge have no such label.

but with a different prefactor.

Experimentally, we measure momentum-resolved tunneling of electrons (fermions with spin) confined to a 1D geometry in the top layer of a GaAs-AlGaAs double-quantum-well structure from/to a two-dimensional electron gas in the bottom layer. We observe a single parabola (which particle-hole asymmetry also affects by increasing relaxation processes [5]) at high energy together with well-resolved spin-charge separation at low energy with appreciable interaction strength (ratio of charge and spin velocities $v_c/v_s \approx 1.4$) [6, 7]. In addition, we can now resolve structure just above k_F that ap-

pears to be the edge of the second-level excitations ($p1b$). However, for higher k we find no sign of the higher-level excitations, implying that their amplitude must have become at least three orders of magnitude weaker than for the first parabola ($h0a$).

Spinless fermions. We study theoretically the model of interacting Fermi particles without spin in 1D,

$$H = \int_{-\frac{L}{2}}^{\frac{L}{2}} dx \left(-\frac{1}{2m} \psi^\dagger(x) \Delta \psi(x) - UL \rho(x)^2 \right), \quad (1)$$

where the field operators $\psi(x)$ satisfy the Fermi commutation relations, $\{\psi(x), \psi^\dagger(x')\} = \delta(x-x')$, $\rho(x) = \psi^\dagger(x) \psi(x)$ is the particle density operator, and m is the bare mass of a single particle. Below we consider the periodic boundary condition, $\psi(x+L) = \psi(x)$, restrict ourselves to repulsive interaction $U > 0$ only, and take $\hbar = 1$.

In the Bethe ansatz approach the model in Eq. (1) is diagonalised by N -particle states parameterised with sets of N quasimomenta k_j that satisfy the non-linear equations $\mathcal{L}k_j - 2 \sum_{l \neq j} \varphi_{jl} = 2\pi I_j$ [8], where $e^{i2\varphi_{ll'}} = -(e^{i(k_l+k_{l'})} + 1 - 2mUe^{ik_l}) / (e^{i(k_l+k_{l'})} + 1 - 2mUe^{ik_{l'}})$ are the scattering phases and I_j are sets of non-equal integer numbers. The dimensionless length of the system $\mathcal{L} = L/\mathcal{R}$ is normalised by the short length-scale \mathcal{R} which is introduced using a lattice (with next-neighbor interaction) as the lattice parameter (and interaction radius) \mathcal{R} that provides microscopically an ultraviolet cutoff for the theory. The latter procedure at high energy is analogous to the point-splitting technique [9] at low energy. For a small \mathcal{R} the scattering phases become linear functions of quasimomenta making the non-linear Bethe-ansatz equations a linear system of equations [10]. Solving them for $\mathcal{L} \gg 1$ via perturbation theory up to the first subleading order in $1/\mathcal{L}$ we obtain

$$k_j = \frac{2\pi I_j}{\mathcal{L} - \frac{mUN}{mU+1}} - \frac{mU}{mU+1} \sum_{l \neq j} \frac{2\pi I_l}{\left(\mathcal{L} - \frac{mUN}{mU+1}\right)}. \quad (2)$$

The corresponding eigenenergy and total momentum (protected by the translational invariance of the system) are $E = \sum_j k_j^2 / (2m)$ and $P = \sum_j k_j$.

The response of a many-body system to a single-particle excitation at momentum k and energy ε is described by a spectral function that, in terms of the eigenstates, reads as [11] $A(k, \varepsilon) = \mathcal{L} \sum_f \left[|\langle f | \psi^\dagger(0) | 0 \rangle|^2 \delta(\varepsilon - E_f + E_0) \delta(k - P_f) + |\langle 0 | \psi(0) | f \rangle|^2 \delta(\varepsilon + E_f - E_0) \delta(k + P_f) \right]$, where E_0 is the energy of the ground state $|0\rangle$, and P_f and E_f are the momenta and the eigenenergies of the eigenstates $|f\rangle$; all eigenstates are assumed normalised. We now turn to calculation of the form factors using the algebraic form of the Bethe ansatz [11].

| | $x = 0$ | $x = 1$ |
|----------|--|--|
| pxa | — | 1 |
| hxa | 1 | — |
| pxb | $\frac{16Z^2 k_F^2 k^2}{(k^2 - (k_F + \gamma)^2)^2}$ | $\frac{4Z^2 \gamma^2 (k - k_F + \frac{3}{2}\gamma)^2}{(k - k_F + \gamma)^2 (k - k_F + 2\gamma)^2}$ |
| $pxb(l)$ | $\frac{4Z^2 (k_F + k)^2}{k_F^2}$ | — |
| $pxb(r)$ | $\frac{4Z^2 (k_F - k)^2}{k_F^2}$ | — |
| hxb | — | $\frac{4Z^2 (3k_F - k - \gamma)^2 (k_F + k)^2}{k_F^2 (k - k_F + \gamma)^2}$ |
| $hxb(l)$ | $\frac{4Z^2 \gamma^2}{(k + k_F + 2\gamma)^2}$ | $\frac{Z^2 k_F^2 k^2}{((k + \gamma)^2 - k_F^2)^2}$ |
| $hxb(r)$ | $\frac{4Z^2 \gamma^2}{(k - k_F - 2\gamma)^2}$ | — |

Table I. Spectral weights along the a - and the b -modes for $-k_F < k < k_F$ ($k_F < k < 3k_F$) labeled by $x = 0(1)$. Terminology is the same as in Fig. 1 and $\gamma = 2\pi/\mathcal{L}$.

To proceed we borrow results from Heisenberg chains: the normalisation of Bethe states was obtained in Ref. 12 and the matrix elements were obtained [13] using Slavnov's formula for scalar products [14] and Drinfeld twists [15] to represent the field operators in the basis of Bethe states. The anti-commutativity of Fermi particles at different positions can be easily added by introducing a fermionic basis for auxiliary space in the construction of the algebraic Bethe ansatz [16], which results in a determinant expression for $\langle f | \psi^\dagger(0) | 0 \rangle$. For a small \mathcal{R} , which corresponds to low particle density we obtain [17]

$$|\langle f | \psi^\dagger(0) | 0 \rangle|^2 = \frac{Z^{2N}}{\mathcal{L}} \frac{\prod_j (k_j^0 - P_f)^2}{\prod_{i,j} (k_j^f - k_i^0)^2} \prod_{i < j} (k_j^0 - k_i^0)^2 \prod_{i < j} (k_j^f - k_i^f)^2, \quad (3)$$

where $Z = mU / (mU + 1) / (\mathcal{L} - NmU / (1 + mU))$ and k_j^f and k_j^0 are quasimomenta of the eigenstate $|f\rangle$ and the ground state $|0\rangle$.

This result is singular when one or more quasimomenta of an excited state coincide with that of the ground state. The divergences occur in the leading order of Eq. (2) but the first subleading order provides a cutoff within the theory cancelling a power of $Z^2 \sim \mathcal{L}^{-2}$ per singularity; when N quasimomenta k_j^f coincide with k_j^0 , Eq.(3) gives $\mathcal{L} |\langle f | \psi^\dagger(0) | 0 \rangle|^2 = 1$. We label the many-body excitations by the remaining powers of \mathcal{L}^{-2} [18], e.g. $p0b$: $p(h)$ indicates the particle (hole) sector, $0(1)$ encodes the range of momenta $-k_F < k < k_F$ ($k_F < k < 3k_F$), and a, b, c reflect the terms \mathcal{L}^{-2n} with $n = 0, 1, 2$. All simple modes, formed by single particle- and hole-like excitations of the ground state k_j^0 , are presented in Fig. 1 and the spectral function along them is evaluated in Table I. Note that the thermodynamic limit involves both $\mathcal{L} \rightarrow \infty$ and the particle number $N \rightarrow \infty$ and the finite combination N/\mathcal{L} ensures that the spectral weight of

sub-leading modes, e.g. the modes $p0b$, $h1b$, and $h1b(r)$, is still apparent in the infinite system.

Excitations around the strongest a -modes have an additional electron-hole pair in their quasimomenta, which introduces an extra factor of \mathcal{L}^{-2} ,

$$|\langle f|\psi^\dagger(0)|0\rangle|^2 = \frac{Z^2 (k_2^f - k_1^f)^2 (k_1^0 - P_f)^2}{\mathcal{L} (k_1^f - k_1^0)^2 (k_2^f - k_1^0)^2}. \quad (4)$$

The energies of the electron-hole pairs themselves are regularly spaced around the Fermi energy with slope v_F . However, degeneracy of the many-body excitations due to the spectral linearity makes the level spacings non-equidistant. Using a version of the spectral function smoothed over energy, $\bar{A}(\varepsilon) = \int_{-\varepsilon_0/2}^{\varepsilon_0/2} d\varepsilon A(\varepsilon + \varepsilon, k) / \varepsilon_0$ where ε_0 is a small energy scale, we obtain $\bar{A}(\varepsilon) = Z^2 2k_F (3k^2 + k_F^2) / (m\gamma K) (\varepsilon_{h0a} - \varepsilon)^{-1} \theta(\varepsilon_{h0a} - \varepsilon)$ and $\bar{A}(\varepsilon) = Z^2 (k + \text{sgn}(\varepsilon - \varepsilon_{p1a(l)}) k_F)^3 / (m\gamma K) |\varepsilon - \varepsilon_{p1a(l)}|^{-1}$ [20], where $\gamma = 2\pi/\mathcal{L}$ and the dispersion of the a -modes is parabolic $\varepsilon_{h0a}(k) = \varepsilon_{p1a(l)}(k) = k^2/(mK)$ with the mass renormalised by the Luttinger parameter K , around the $h0a$ and $p1a(l)$ modes. The exponent -1 coincides with the prediction of the mobile impurity model [4] where the spectral edge is an a -modes, $h0a$.

Excitations around b -modes belong to the same level of hierarchy as the modes themselves, Eq. (4), giving a more complicated shape of the spectral function. Let us focus on one mode, $p0b$. It has a new power-law behaviour characterised by an exponent changing with k from $\bar{A}(\varepsilon) \sim (\varepsilon - \varepsilon_{p0b})^3$ for $k = 0$ to $\bar{A}(\varepsilon) \sim \text{const} - (\varepsilon - \varepsilon_{p0b})$ for $k \approx k_F$, where $\varepsilon_{p0b}(k) = k_F^2/(mK) - k^2/(mK)$. This is essentially different from predictions of the mobile-impurity model. Here we observe that the phenomenological model in Refs. 21 is correct only for the a -mode spectral edge but higher-order edges require a different field-theoretical description. The density of states is linear, $\nu(\varepsilon) \sim (\varepsilon - \varepsilon_{p0b})$, but level statistics varies from having a regular level spacing (for k commensurate with k_F) to an irregular distribution (for incommensurate k), which is another microscopic difference between a - and b -modes.

Now we use the result in Eq. (3) to calculate another observable, the local density of states. It is independent of position for translationally invariant systems and, in term of eigenmodes, is [11, 22] $\rho(\varepsilon) = \mathcal{L} \sum_f \left[|\langle f|\psi^\dagger(0)|0\rangle|^2 \delta(\varepsilon - E_f + E_0) + |\langle 0|\psi(0)|f\rangle|^2 \delta(\varepsilon + E_f - E_0) \right]$. The leading contribution for $\varepsilon > 0$ comes from a -modes, $\rho(\varepsilon) = \theta(\varepsilon) \sqrt{2mK/\varepsilon}$, which gives the same $1/\sqrt{\varepsilon}$ functional dependence as the free-particle model—see red line in Fig. 2. Around the Fermi energy the Tomonaga-Luttinger model predicts power-law suppression of

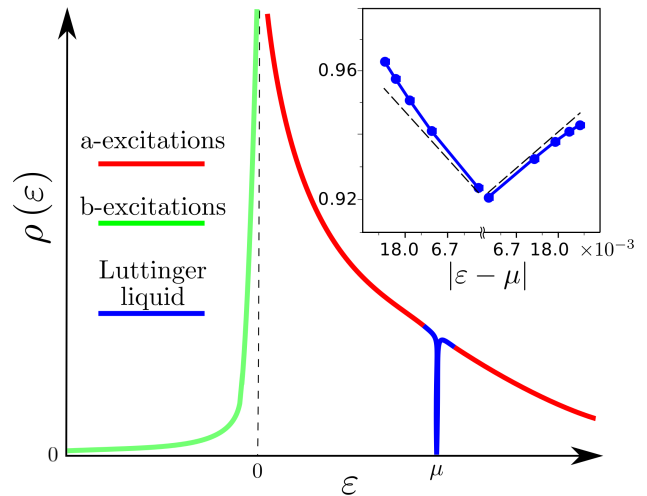


Figure 2. The local density of states for spinless fermions: red and green lines show the contribution of a - and b -excitations and the blue line indicates the Luttinger-liquid regime. Inset is a log-log plot around the Fermi energy: the blue points are numerical data for $N = 71$, $L = 700$, $mV = 6$ giving $K = 0.843$, and the dashed line is $\rho(\varepsilon) = \text{const} |\varepsilon - \mu|^{(K+K^{-1})/2-1}$.

$\rho(\varepsilon) \sim |\varepsilon - \mu|^{(K+K^{-1})/2-1}$ [2] (blue region in Fig. 2) signaling that the leading-order expansion in the $\mathcal{L} |\langle f|\psi^\dagger(0)|0\rangle|^2 = 1$ result is insufficient. We evaluate $\rho(\varepsilon)$ numerically in this region using determinant representation of the form factors for the lattice model instead of Eq. (3) (inset in Fig. 2) [23]. Away from the point $\varepsilon = \mu$ the particle-hole symmetry of the Tomonaga-Luttinger model is broken by the curvature of the dispersion of the a -modes. For $\varepsilon < 0$ the leading contribution to $\rho(\varepsilon)$ comes from b -modes. Using Eq. (4) we obtain $\rho(\varepsilon) = 2Z^2 k_F^2 / (\gamma\mu K) [2(1 - 3|\varepsilon|/\mu) \sqrt{\mu} \cot^{-1}(\sqrt{|\varepsilon|/\mu}) / \sqrt{|\varepsilon|+6}] \theta(-\varepsilon)$, which contains another Van Hove singularity $\rho(\varepsilon) = 2\pi Z^2 k_F^2 / (\gamma K \sqrt{\mu\varepsilon})$ at the bottom the conduction band (green line in Fig. 2).

Fermions with spin. We study experimentally spin-unpolarised electrons in a high-mobility GaAs-AlGaAs double-quantum-well structure with electron density around $2 \times 10^{15} \text{ m}^{-2}$ in each layer. Electrons in the top layer are confined to a 1D geometry by split gates. Our devices contain an array of ~ 500 highly regular wires to boost the signal from 1D-2D tunneling. The small lithographic width of the wires, $\sim 0.18 \mu\text{m}$, provides a large energy spacing between the first and second 1D subbands, allowing a wide energy window for electronic excitations in the single-subband case—see device schematic in Fig. 3f and more details in Ref. 7.

The 2DEG in the bottom layer is separated from the wires by a $d = 14 \text{ nm}$ tunnel barrier (giving a spacing between the centres of the wavefunctions of $d = 36 \text{ nm}$). It is used as a controllable injector or collector of elec-

trons for the 1D system [24]. A sharp spectral feature in the density of states of the 2DEG produced by integration over momenta in the direction perpendicular to the wires can be shifted in energy by a dc-bias between the layers, in order to probe different energies. Also, an in-plane magnetic field B applied perpendicular to the wires changes the longitudinal momentum in the tunneling between layers by $\Delta k = eBd/\hbar$, where e is the electronic charge, and so probes the momentum. Together they reveal the dispersion relation of states in each layer. In this magnetic field range the system is still within the regime of Pauli paramagnetism for the electron densities in our samples.

We have measured the tunneling conductance G between the two layers (see Fig. 3f) in detail in a wide range of voltage and magnetic field, corresponding to a large portion of the 1D spectral function from $-k_F$ to $3k_F$ and from -2μ to 2μ (Fig. 3a). At low energy we observe spin-charge separation [7]. The slopes of the charge (C) and spin (S) branches—black dashed lines—are $v_c \approx 2.03 \times 10^5 \text{ms}^{-1}$ and $v_s \approx 1.44 \times 10^5 \text{ms}^{-1}$, respectively, with $v_c/v_s \approx 1.4 \pm 0.1$. This large ratio, together with a strong zero-bias suppression of tunneling [7], confirms that our system is in the strongly interacting regime.

Unavoidable ‘parasitic’ (‘p’) tunneling from narrow 2D regions connecting the wires to the injector constriction [7], superimpose a set of parabolic dispersions, marked by magenta and blue dotted lines in Fig. 3a [25], on top of the 1D-2D signal. Apart from them we observe a single 1D parabola, marked by the solid green line in Fig. 3a, which extends from the spin-excitation branch at low energy. The position of its minimum gives the 1D chemical potential $\mu \approx 3 \text{meV}$ and its crossings with the line $V_{dc} = 0$, corresponding to momenta $-k_F$ and k_F , give the 1D Fermi momentum $k_F \approx 8 \times 10^7 \text{m}^{-1}$.

All other edges of the 1D spectral function are constructed by mirroring and translation of the hole part of the observable 1D dispersion, dashed green and blue lines in Figs. 3. We observe a distinctive feature in the region just above the higher $V_{dc} = 0$ crossing point (k_F): the 1D parabola, instead of just continuing along the non-interacting parabola, broadens, with one boundary following the parabola ($p1a(l)$) and the other bending around, analogous to the replica $p1b$. This is observed in samples with different wire designs and lengths ($10 \mu\text{m}$ (a-d), and $18 \mu\text{m}$, (e)) and at temperatures from 100 mK up to at least 300 mK. The strength of the $p1b$ feature decreases as the B field increases away from the crossing point analogously to that for spinless fermions in Table I, though it then passes a ‘p’ parabola. (b) and (c) show the replica feature for two different positions of the ‘p’ parabolae using a gate above most of the ‘p’ region, showing that the replica feature is independent of the ‘p’ tunneling. G is plotted in (d) on cuts along the V_{dc} axis of (a) at various fields B from 3 to 4.8 T; between the ‘+’

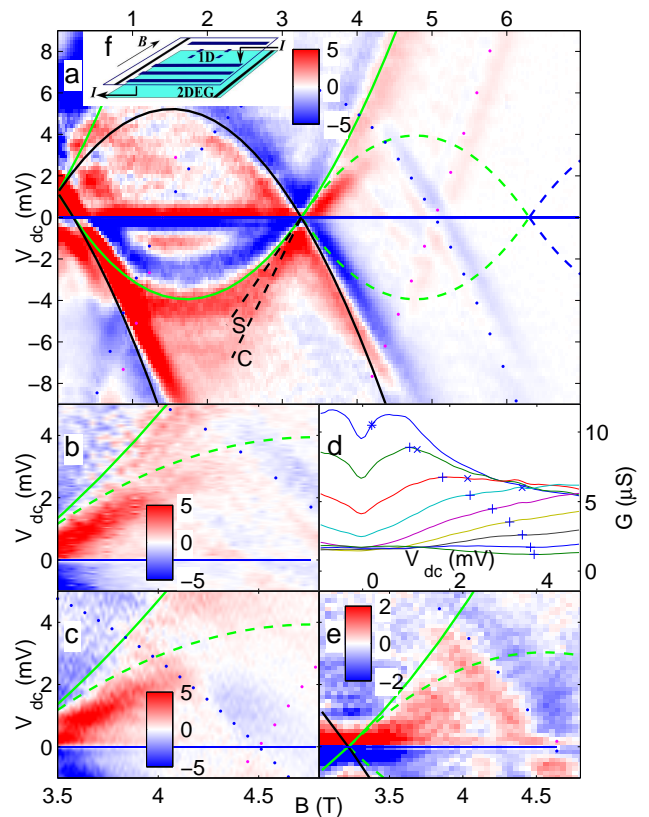


Figure 3. Measurement of the tunneling differential conductance $G = dI/dV$ for two samples, each consisting of a set of identical wires of length $L = 10 \mu\text{m}$ (a-d) and $L = 18 \mu\text{m}$ (e), sketched in inset f. (a) Intensity plot of dG/dV_{dc} in the range $(-k_F..3k_F, -2\mu..2\mu)$. The green solid line marks a -modes, dashed green lines, b -modes and dashed blue, c -modes (as in Fig. 1); dotted magenta and blue lines are parasitic 2D dispersions. Spin (S) and charge (C) modes are indicated with black dashed lines. $T = 300 \text{mK}$. (b) Enlargement of the replica feature in (a) just above k_F . It appears as a pale band (slowly varying G) between the two green curves, after a red region (sharp rise in G). (c) The same as in (b), but with the gate voltage over most of the parasitic (‘p’) region changed to move the ‘p’ parabolae. (d) G vs V_{dc} at various fields B from 3 to 4.8 T (from (a)); ‘+’ and ‘x’ symbols on each curve indicate, respectively, the voltages corresponding to the dashed and solid ($p1b$ and $p1a(l)$) green lines in (a) and (b), showing the enhanced conductance between the two. (e) dG/dV_{dc} for a second device, at $T < 100 \text{mK}$. The replica feature is similar to that shown in (b) and (c) for the other sample.

and ‘x’ symbols on each curve is the region of enhanced conductance characteristic of the replica $p1b$. The amplitude of the feature dies away rapidly, and beyond the ‘p’ parabolae, we have measured up to 8 T with high sensitivity, and find no measurable sign of any feature above the experimental noise threshold. This places an upper limit on the amplitude of any replica away from k_F of at least three orders of magnitude less than that of the a -mode ($h0a$).

Making an analogy with the microscopic theory for spinless fermions above, we estimate the ratio of signals around different spectral edges using the 1D Fermi wavelength, $\lambda_F \approx 80$ nm for our samples, as the short-range scale. The amplitude of signal from the second (third)-level excitations is predicted to be smaller by a factor of more than $\lambda_F^2/L^2 = 6 \times 10^{-5}$ ($\lambda_F^4/L^4 = 4 \times 10^{-9}$), where the length of a wire is $L = 10$ μ m. These values are at least an order of magnitude smaller than the noise level of our experiment. Thus, our observations are consistent with the mode hierarchy picture for fermions.

In conclusion, we have shown that a hierarchy of modes can emerge in an interacting 1D system controlled by the system length. The dominant mode for long systems has a parabolic dispersion, like that of a renormalised free particle, in contrast with distinctly non-free-particle-like behaviour at low energy governed by the Tomonaga-Luttinger model. Experimentally we find a clear feature resembling the second-level excitations, which dies away at high momentum.

We acknowledge financial support from the UK EPSRC through Grant No. EP/J01690X/1 and EP/J016888/1.

[1] P. Nozieres, *Theory of Interacting Fermi Systems* (Addison-Wesley, 1997).
 [2] T. Giamarchi, *Quantum physics in one dimension* (Clarendon press 2003).
 [3] A. Imambekov, T. L. Schmidt, and L. I. Glazman, *Rev. Mod. Phys.* **84**, 1253 (2012).
 [4] O. Tsypliyatyeu and A. J. Schofield, *Phys. Rev. B* **88**, 115142 (2013).
 [5] G. Barak, H. Steinberg, L. N. Pfeiffer, K. W. West, L. Glazman, F. von Oppen, and A. Yacoby, *Nature Physics* **6**, 489 (2010).
 [6] O. M. Auslaender, A. Yacoby, R. de Picciotto, K. W. Baldwin, L. N. Pfeiffer, and K. W. West, *Science* **295**, 825 (2002).
 [7] Y. Jompol, C. J. B. Ford, J. P. Griffiths, I. Farrer, G. A. C. Jones, D. Anderson, D. A. Ritchie, T. W. Silk, A. J.

Schofield, *Science* **325**, 597 (2009).
 [8] V. E. Korepin, N. M. Bogoliubov, A. G. Izergin, *Quantum inverse scattering methods and correlation functions* (Cambridge University Press, 1993).
 [9] J. von Delft and H. Schoeller, *Ann. Phys.* **7**, 225 (1998).
 [10] O. Tsypliyatyeu and A. J. Schofield, *Phys. Rev. B* **90**, 014309 (2014).
 [11] A. A. Abrikosov, L. P. Gorkov, I. E. Dzyaloshinski, *Methods of quantum field theory in statistical physics* (Dover Publications, New York, 1975).
 [12] M. Gaudin, B. M. McCoy, and T. T. Wu, *Phys. Rev. D* **23**, 417 (1981).
 [13] N. Kitanine, J.M. Maillet, V. Tetras, *Nucl. Phys. B* **554**, 647 (1999); *ibid. Nucl. Phys. B* **567**, 554 (2000).
 [14] N. A. Slavnov, *Theor. Math. Phys.* **79**, 502 (1989).
 [15] V. G. Drinfeld, *Sov. Math. Dokl.* **28**, 667 (1983).
 [16] F. Gohmann and V. E. Korepin, *J. Phys. A: Math. Gen.* **33**, 1199 (2000); K. Motegi and K. Sakai, *Nucl. Phys. B* **793**, 451 (2008).
 [17] The result in Eq. (3) was verified by direct summation over spatial variables for up to $N = 3$ particles and details of its derivation will be published elsewhere.
 [18] A similar hierarchy of excitations is observed in numerical studies of spin chains at large fillings, *e.g.* [19], for which Eq. (3) is not applicable.
 [19] J.-S. Caux and J. M. Maillet, *Phys. Rev. Lett.* **95**, 077201 (2005).
 [20] The exponent -1 is valid while the level spacings remain regular, $|\varepsilon - \varepsilon_{p1a(h0a)}| \lesssim k_F^2/(mK)$. Below the $p1a$ mode, the spectral edge gives an additional restriction, $\varepsilon_{p1a} - \varepsilon \lesssim (k_F - k)^2/(mK)$.
 [21] M. Pustilnik, M. Khodas, A. Kamenev, and L. I. Glazman, *Phys. Rev. Lett.* **96**, 196405 (2006); A. Imambekov and L. I. Glazman, *Phys. Rev. Lett.* **102**, 126405 (2009).
 [22] It is equivalent to conventional definition, $\rho(x, \varepsilon) = -\text{Im}[\int dt e^{-i\varepsilon t} G(x, x, t)] \text{sgn}(\varepsilon - \mu)/\pi$, using the two point correlation function $G(x, x', t) = -i \langle T(e^{-iHt} \psi(x) e^{iHt} \psi^\dagger(x')) \rangle$ at zero temperature.
 [23] The regions of validity of the Tomonaga-Luttinger model and Eq. (3) have a large overlap around $\varepsilon = \mu$ since power-law suppression of $\rho(\varepsilon)$ has a very small exponent due to only small deviations from $K = 1$ for arbitrary short-range interactions between spinless fermions.
 [24] A. Altland, C. H. W. Barnes, F. W. J. Hekking, A. J. Schofield, *Phys. Rev. Lett.* **83**, 1203 (1999).
 [25] All the parabolae have been modified to attempt to take into account the capacitance between the layers, see details in Ref. 7.